A Study of Deformable-Mirror Performance Versus Actuator Distribution Using an Influence-Function Model

D. J. Hoppe[1]

A study of deformable-mirror performance versus the number of actuators on the mirror and their locations is summarized. Influence functions are used to model the effect of the actuators on the deformable mirror's shape. This simplified model is sufficient for the purpose of this study. It has the advantage that no finite-element model for the mirror is required, and therefore a large number of scenarios may be studied with minimal overhead. The first case studied concerns compensation for the measured distortion of DSS 13 at an elevation angle of 12.7 deg. Results are given for distortion compensation versus deformable-mirror location and the number of actuators on the mirror. A rectangular grid of actuators at various densities is studied along with an actuator configuration specifically designed for this distortion. This actuator configuration is presently used in the experimental deformable mirror. Results are also presented for compensation versus elevation angle using a distortion model based on measurements taken at DSS 43.

I. Introduction

Gain loss due to gravity distortion effects on a large reflector antenna can become significant for a sufficiently high operating frequency [1]. This is certainly the case for the DSN 70-m antennas operating near 32 GHz (Ka-band). One approach for restoring the lost gain is to insert a deformable mirror in the beam path that can be distorted to counteract the main-reflector distortions and restore the lost efficiency. Recent demonstrations have indeed demonstrated gain recovery on DSS 14 using this approach [2].

There are three major factors affecting the performance of a deformable-mirror system. The first factor that will limit performance is that perfect knowledge of the true main-reflector shape is required in order to obtain perfect compensation from the deformable mirror. Recently a campaign was initiated to measure the surface of the DSN 70-m antennas versus elevation angle directly using a ranging theodolite [3]. In addition to the measurement errors themselves, which are discussed in [3], interpolation errors occur when a finite number of measurements are used to predict the surface error at any arbitrary elevation angle.

The second limitation, placement of the deformable mirror in the path, was the subject of a previous article [4]. As the field propagates away from the distorted main reflector, the phase distortions are

[1] Communications Ground Systems Section.

The research described in this publication was carried out by the Jet Propulsion Laboratory, California Institute of Technology, under a contract with the National Aeronautics and Space Administration.

partially converted into amplitude distortions through the radiation process. Therefore, at an arbitrary position in the beam path, both an amplitude and a phase correction are required. The deformable mirror can provide only a phase correction and will have limited performance at any arbitrary location due to the amplitude distortion present there. These effects are described in detail in [4].

In general, an infinite number of actuators are required on the deformable mirror in order to produce an arbitrary deformation. The finite number of degrees of freedom in the plate due to a finite number of actuators is the third limitation. This article addresses this limitation. Influence functions [5] are used to model the actuator's effect on the mirror shape. This simple model is satisfactory for determining the effects of actuator spacing on distortion compensation without the need for a detailed finite-element model for the mirror. If an operational deformable-mirror system is to be deployed on the 70-m antennas, an analysis similar to that presented here needs to be performed to determine the optimum number of actuators to be employed. The optimum number of actuators will depend on how closely the mirror can be placed to the ideal image position in the beam path, a model for mirror cost versus number of actuators, and the expected performance. With the completion of the work described in this article, all of the tools are in place to design an operational deformable-mirror system.

The next three sections describe the geometry, coupling theory, and influence-function model for the actuators. Subsequent sections present results for some case studies and conclusions.

II. Geometry

A schematic representation of the case under consideration is shown in Fig. 1. The geometry is identical to that described in [4], where the main and subreflector surfaces are chosen to be the DSS-13 shaped surfaces. A re-imaging ellipse with a focal length of 2.73 m directs the incoming radiation onto the deformable mirror placed a distance dz in front of the feed.

Of primary interest in this article is the ability of this deformable mirror to correct for the main-reflector distortion versus the number of actuators employed. Also of importance is the mirror's position in the beam path, dz. As is discussed in [4], a simple optical analysis shows that optimum performance of the deformable mirror is expected when it is located at the image of the primary mirror. This image forms at a distance $dz = 1$ m.

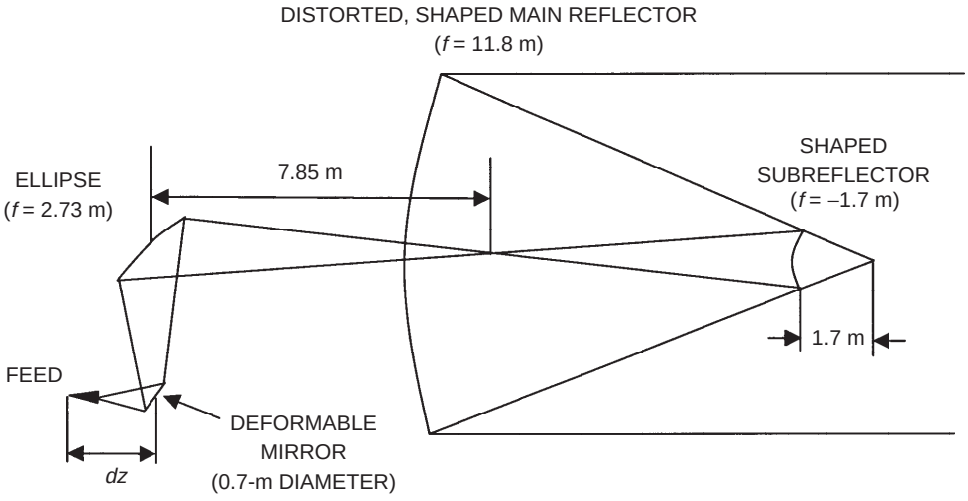

Fig. 1. Geometry for the case study.

III. Coupling Theory

As described in [4], the effectiveness of the deformable mirror is determined by computing a coupling integral over the current on the mirror generated by two different excitations—one for plane-wave incidence, the other for the feed radiation pattern. If the two currents on the deformable mirror generated by these two excitations are complex conjugates of each other, perfect coupling occurs and the feed will radiate with maximum efficiency in the boresight direction. Any difference in phase, amplitude, or polarization between these currents results in an efficiency loss. Definitions of the various efficiency terms and details of the efficiency calculation are given in [4].

As is shown in [4], the overall voltage coupling efficiency may be factored as

$$\eta_{tot} = \eta_A \eta_\phi \eta_{\text{spill}}$$

The spillover efficiency, η_{spill}, can approach unity for a large enough deformable mirror placed anywhere in the beam path. The amplitude efficiency is less than unity if the amplitude patterns of the feed current and plane-wave current are mismatched. The deformable mirror cannot correct for this amplitude mismatch. By deforming the mirror, a phase adjustment may be made to increase the phase efficiency. The distribution between phase and amplitude efficiency depends on the position of the mirror. In order to compute the available efficiency from an idealized, perfectly deformable mirror, the phase efficiency term above is simply replaced by unity. In this study, the limited ability of the actuators to form this ideal, phase-correcting distortion is taken into account. The actuator pressures are varied in order to optimize the coupling integral, approaching the idealized distortion as closely as possible for each actuator configuration. For the purposes of this study, the relationship between the actuator pressures and the deformation of the mirror is described in terms of influence functions that are discussed next.

IV. Influence-Function Theory

For small displacements, the relationship between mirror pressure and displacement may be found by solving Poisson's equation [5]. An analytic solution is available for a circular mirror, constrained to $z = 0$ at the edge. In this case, the deformation $z(r, \phi)$ may be found by convolving the applied pressure with the Green's function for the problem:

$$z(r,\phi) = \frac{a^2}{2\pi T} \int_0^{2\pi} d\phi' \int_0^1 G\left(r, r', \phi, \phi'\right) P\left(r', \phi'\right) r' dr'$$

Here the Green's function is given by

$$G\left(r, r', \phi, \phi'\right) = \ln\left(\frac{1}{r}\right) - \sum_{n=1}^{\infty} \frac{1}{n}\left[\left(rr'\right)^n - \left(\frac{r'}{r}\right)^n\right] \cos\left(n\left(\phi' - \phi\right)\right); r > r'$$

and

$$G\left(r, r', \phi, \phi'\right) = \ln\left(\frac{1}{r'}\right) - \sum_{n=1}^{\infty} \frac{1}{n}\left[\left(rr'\right)^n - \left(\frac{r}{r'}\right)^n\right] \cos\left(n\left(\phi' - \phi\right)\right); r < r'$$

In the above equations, r and r' are normalized to the overall mirror radius; T is the surface tension; and a is the plate radius. The primed coordinates refer to the source point, and the unprimed coordinates to

the point of the deformation. For this study, the radius at which the mirror is constrained was chosen to be very large, at least 10 times the radius containing the actuators. In this way the mirror acts as if it were effectively unconstrained. The finite size of the actuator is modeled by using an array of point sources for each actuator. All point sources modeling a given actuator are constrained to apply the same pressure. In general, several hundred terms are included in the summation appearing in the Green's function.

Once the actuator configuration on the mirror is defined, the relationship between the applied pressure on each actuator and the displacement at any point is fixed and linear. In practice this relationship is stored in a matrix that relates the displacement at the center of each triangle in the mirror model to the actuator pressures. This matrix is computed once and used for all calculations involving that actuator configuration. This greatly increases computation speed, particularly during the numerical optimization of the coupling integral.

V. Results

For the first case in this study, a smoothed version of the distortion obtained using holography at DSS 13 for an elevation angle of 12.7 deg was used. The surface height distortion is plotted in Fig. 2 and is identical to that used in [4]. This distortion was then amplified by factors of two and three in order to evaluate the performance characteristics of the deformable-mirror system for main-reflector distortions resulting in more significant gain loss. All of the physical optics calculations were carried out at 32 GHz.

Figure 3 shows the overall voltage coupling efficiency for the 12.7-deg distortion versus mirror position and a feed gain of 22.37 dBi. Results for mirrors with 4, 12, 32, and 52 actuators placed on a rectangular grid are shown. A fifth deformable mirror, the existing mirror used in previous hardware demonstrations, is also included. It has 16 actuators with a placement optimized for this 12.7-deg distortion, as shown in Fig. 4. Efficiency for a flat plate and the theoretical maximum efficiency are also plotted. The theoretical maximum efficiency is achieved when the phase errors are fully corrected and only amplitude mismatch and spillover contribute. The figure illustrates that 4 actuators are insufficient for improving the efficiency, whereas 12 actuators can provide a substantial improvement. As expected, more actuators provide higher efficiency. The existing mirror, designed for this particular distortion, performs exceptionally well, providing nearly the same compensation as a 32-actuator, square-grid mirror.

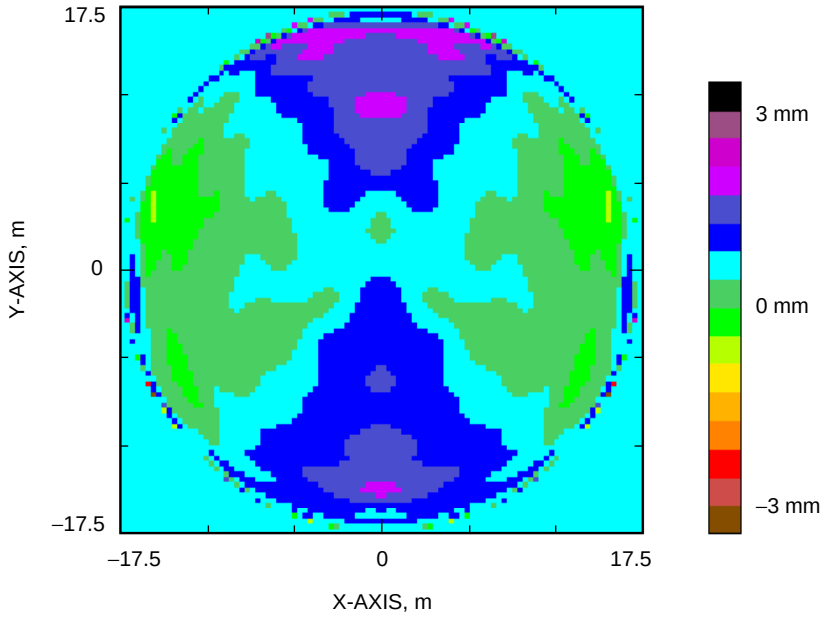

Fig. 2. Nominal main-reflector distortion.

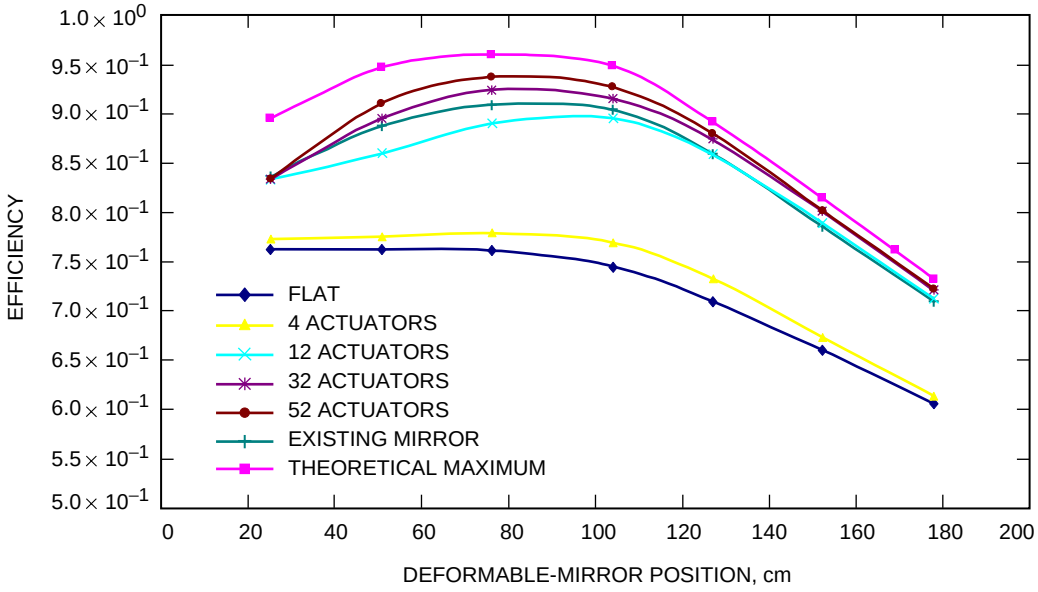

Fig. 3. Deformable-mirror performance, nominal distortion.

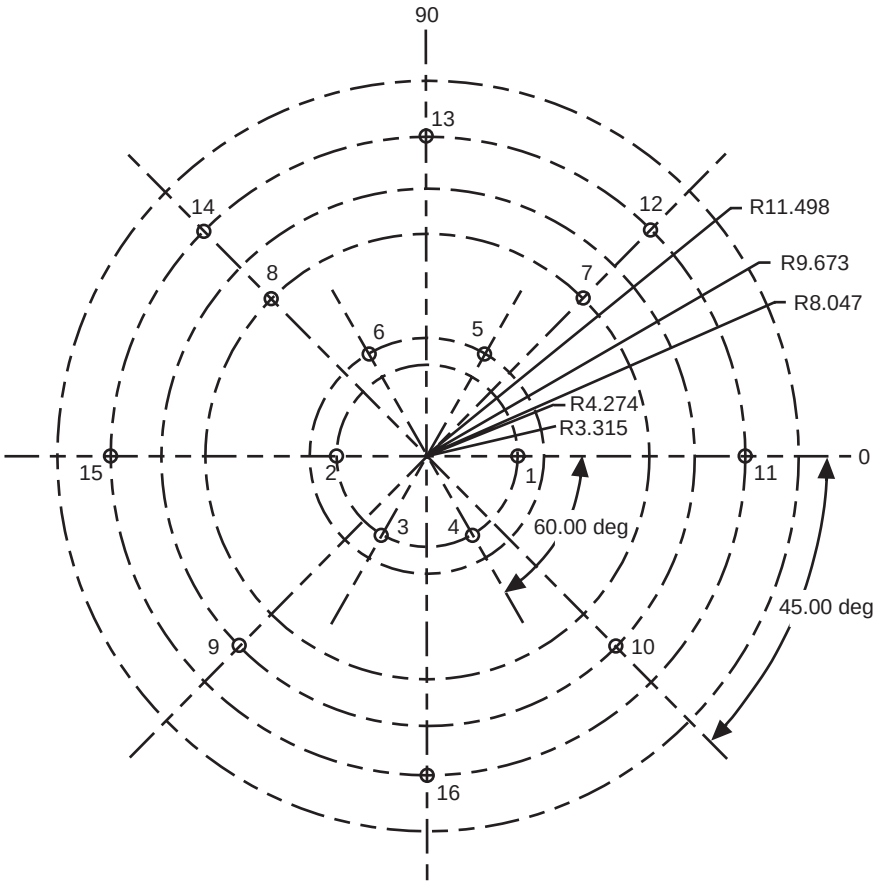

Fig. 4. Actuator placement on the existing deformable mirror.

Figure 5 shows the amplitude distribution due to the feed illumination on the mirror for $dz = 104$ cm, the image location. Figure 6 shows the current amplitude for plane-wave excitation. An excellent match exists for these two amplitude patterns. The phase difference is shown in Fig. 7. The deformable mirror must be distorted to correct for this phase error. As expected, the phase error plot closely resembles the distortion of the main reflector (Fig. 2) at this image location. Figure 8 shows the optimized mirror distortion for the 32-actuator case. The similarity to Fig. 7 is obvious, indicating that 32 actuators are sufficient to provide a high degree of phase correction. At $dz = 104$ cm, the flat-plate efficiency is 74.4 percent; the maximum voltage coupling efficiency is 76.9 percent for 4 actuators, 89.4 percent for 12 actuators, 91.5 percent for 32 actuators, 92.7 percent for 52 actuators, and 90.4 percent for the existing 16-actuator plate; and the theoretical maximum efficiency is 94.8 percent.

Figures 9 through 11 show the voltage coupling efficiency, plane-wave amplitude distribution at $dz = 104$ cm, and the phase error for the case of the 12.7-deg main-reflector distortion doubled in amplitude. As expected, the nominal coupling loss is significantly increased, and more separation is seen between the coupling efficiency for the various deformable-mirror configurations. Figure 10 shows slightly more amplitude distortion in the plane-wave current, and Fig. 11 is essentially an amplified version of Fig. 7. For this case, at $dz = 104$ cm the flat-plate efficiency is 32.9 percent; the maximum efficiency is 40.6 percent for 4 actuators, 76.0 percent for 12 actuators, 83.0 percent for 32 actuators, 86.9 percent for 52 actuators, and 80.2 percent for the existing 16-actuator plate; and the theoretical maximum efficiency is 94.3 percent.

Figures 12 through 14 show results for the 12.7-deg distortion tripled. Further amplitude distortion is indicated in Fig. 13. Figure 14 illustrates the special property of the image location where the phase error is nearly an exact duplicate of the main-reflector distortion. Significant phase wrapping is evident in Fig. 14 due to the large phase errors in this case. For this case, at $dz = 104$ cm the flat-plate efficiency

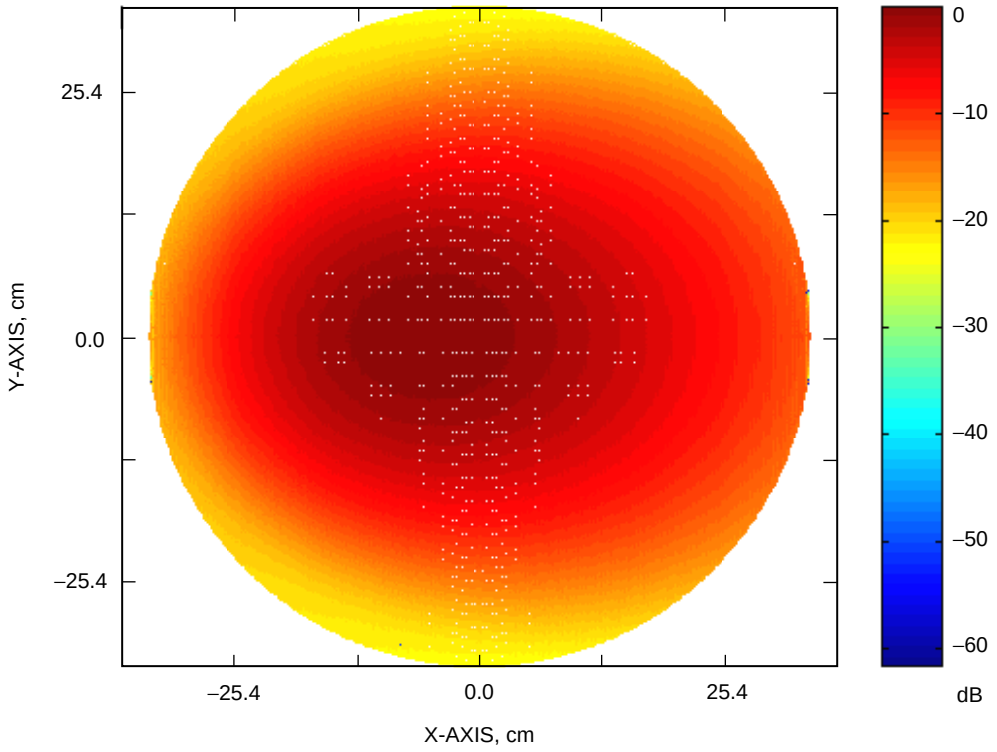

Fig. 5. Mirror current amplitude due to the feed.

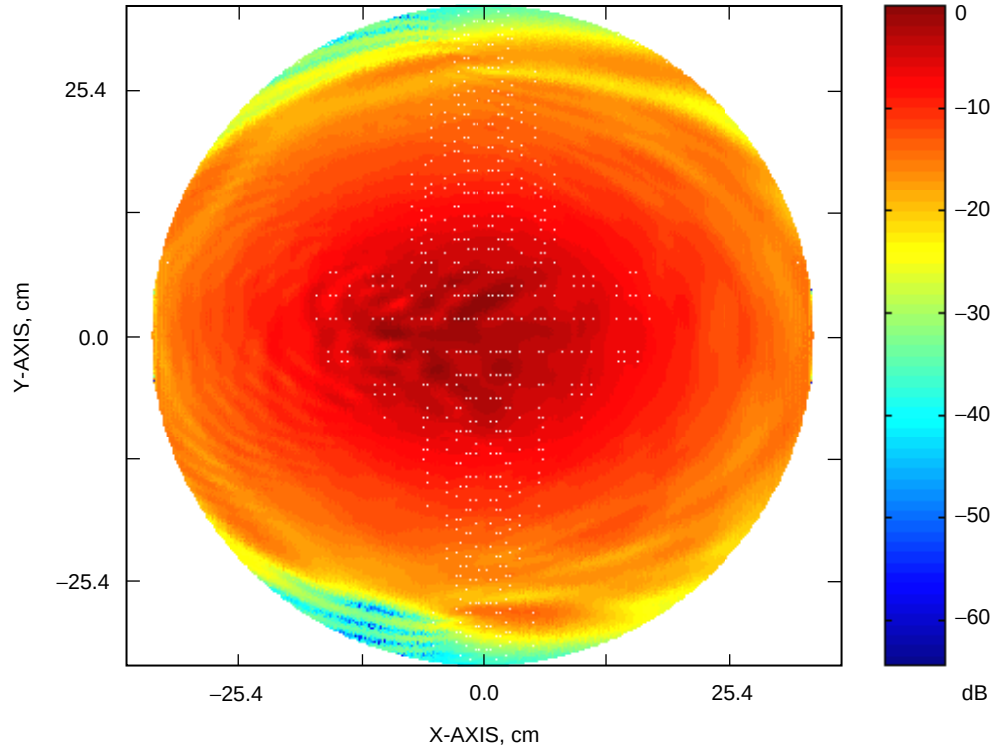

Fig. 6. Mirror current amplitude due to the plane wave, nominal distortion.

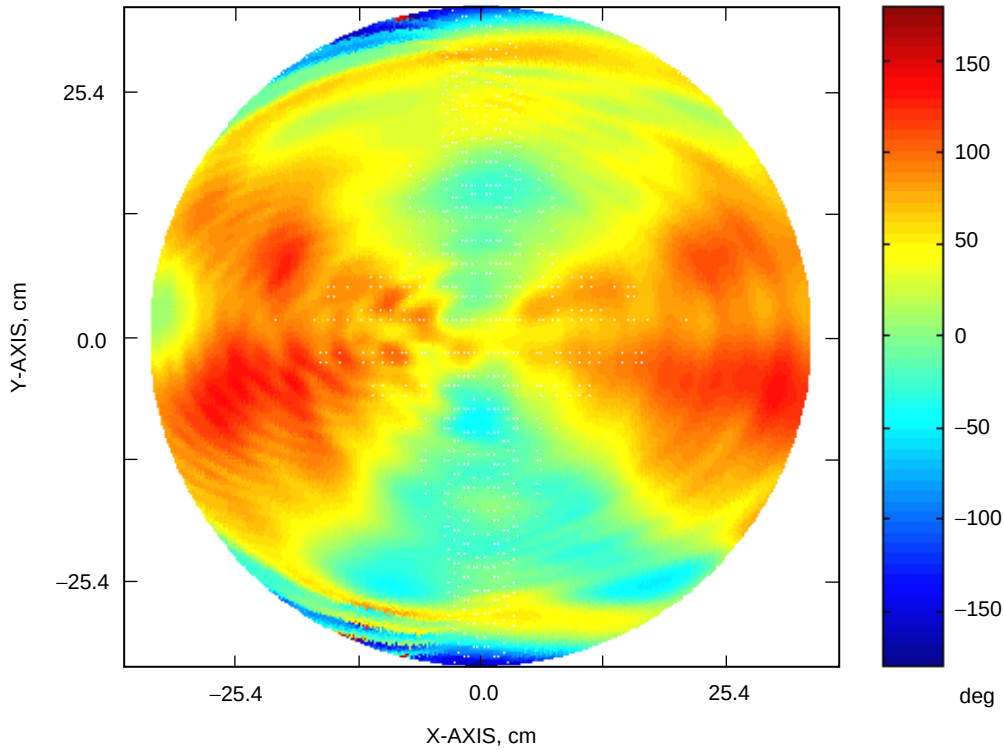

Fig. 7. Mirror current phase error, nominal distortion.

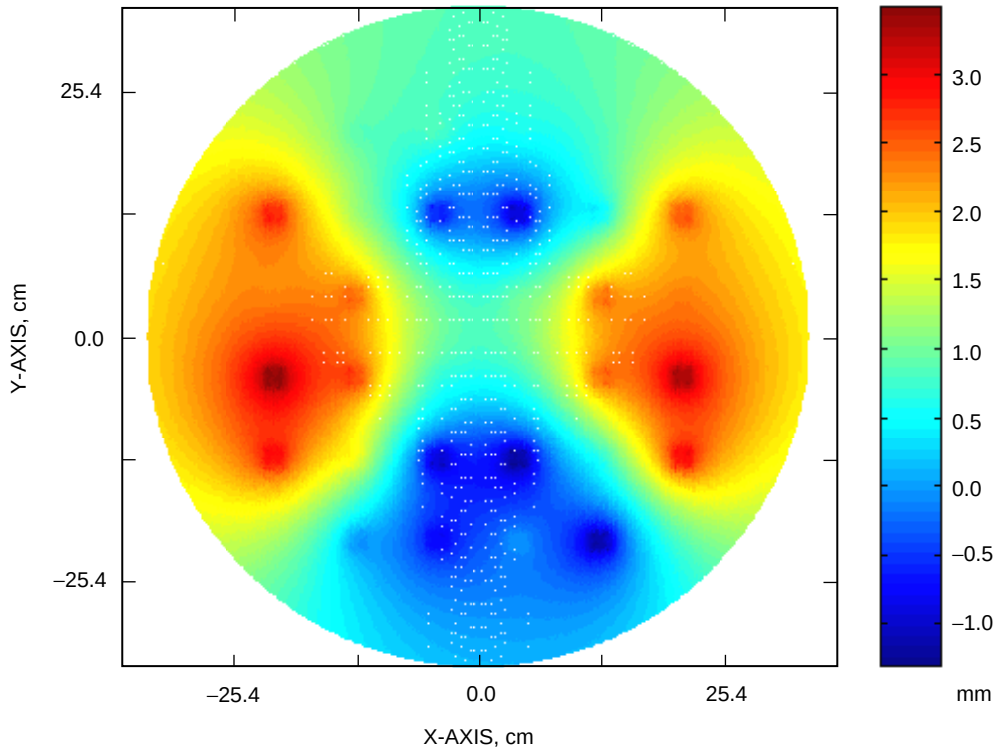

Fig. 8. Deformable mirror shape, 32 actuators, nominal distortion.

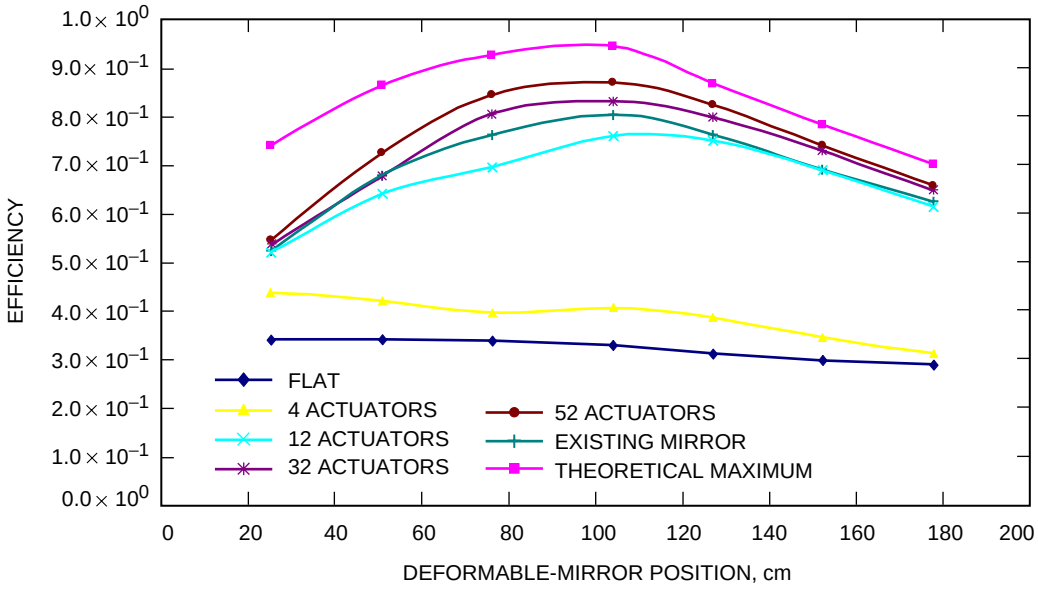

Fig. 9. Deformable-mirror performance, nominal distortion doubled.

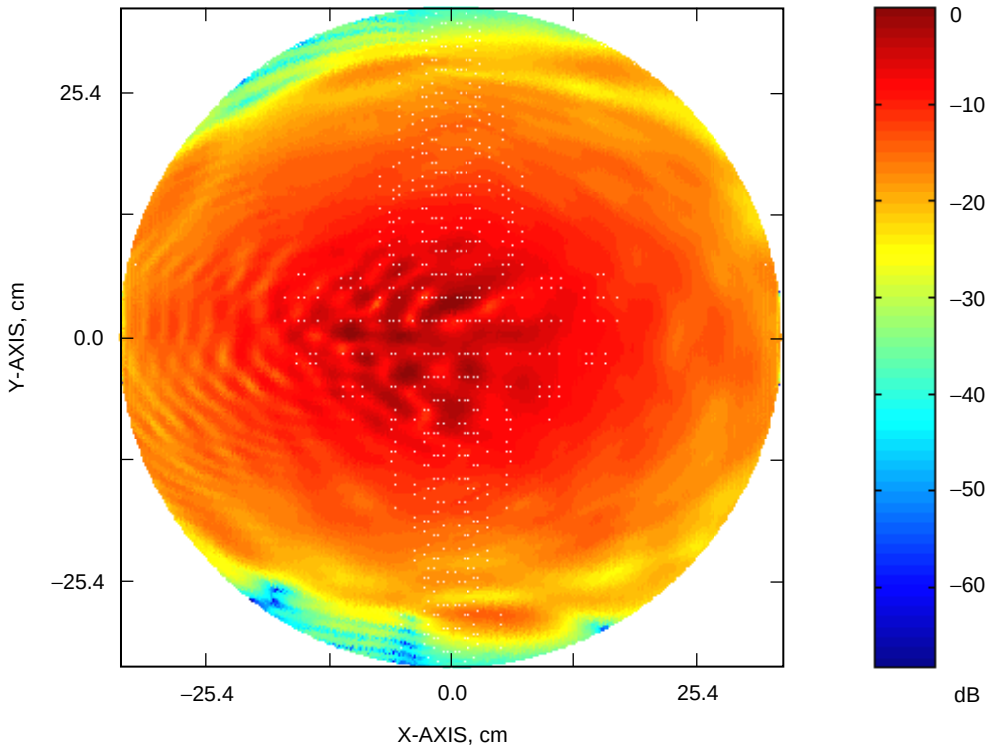

Fig. 10. Mirror current amplitude due to the plane wave, nominal distortion doubled.

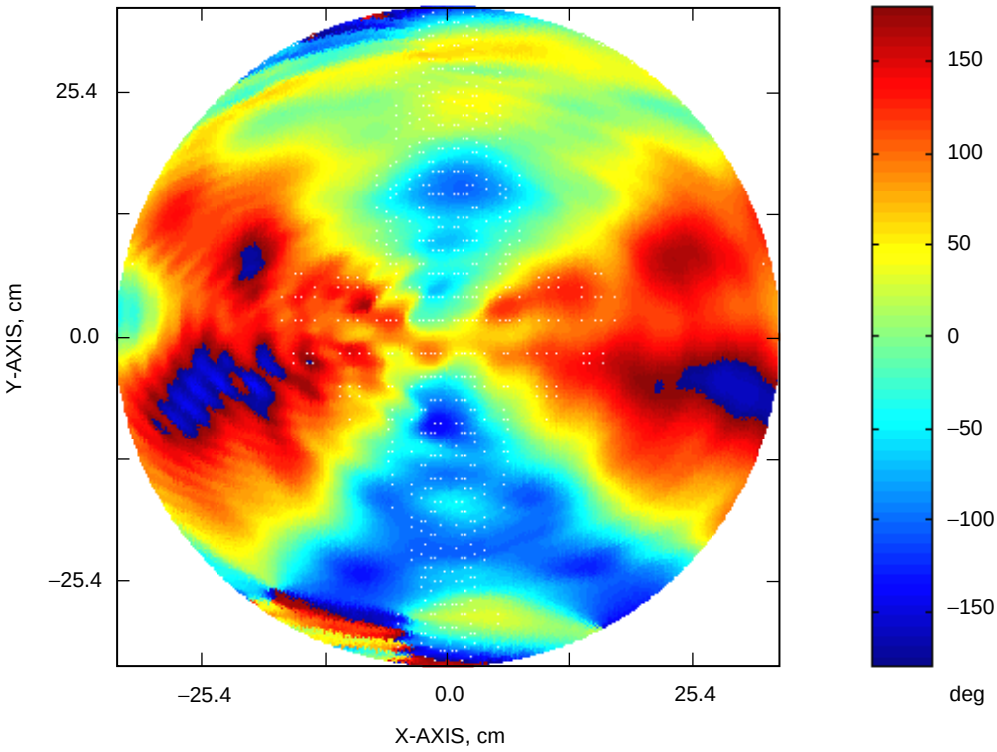

Fig. 11. Mirror current phase error, nominal distortion doubled.

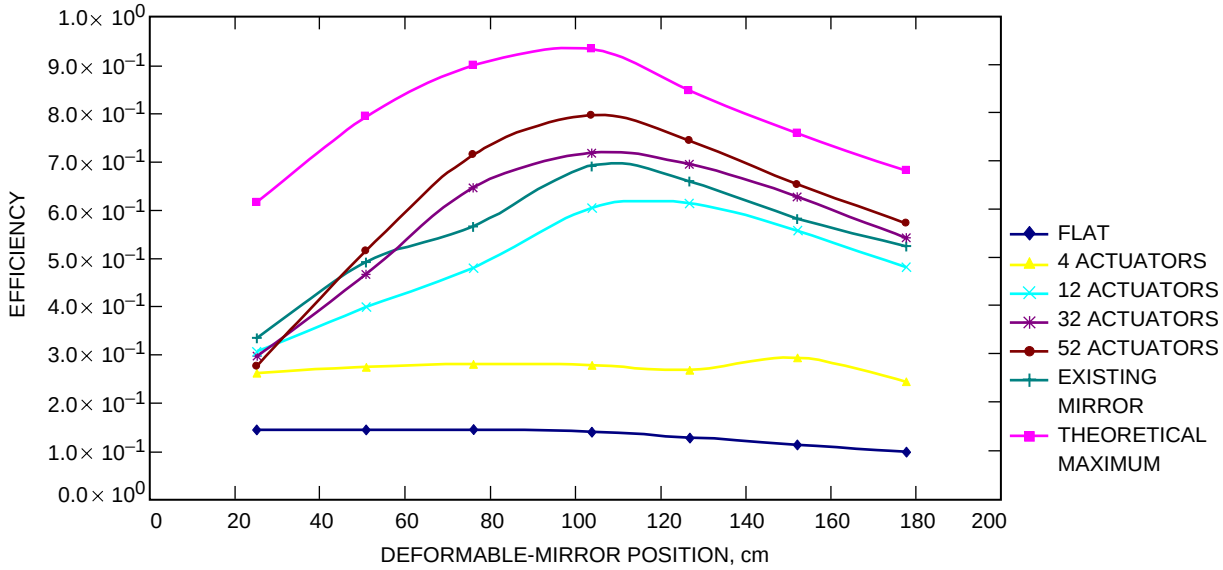

Fig. 12. Deformable-mirror performance, nominal distortion tripled.

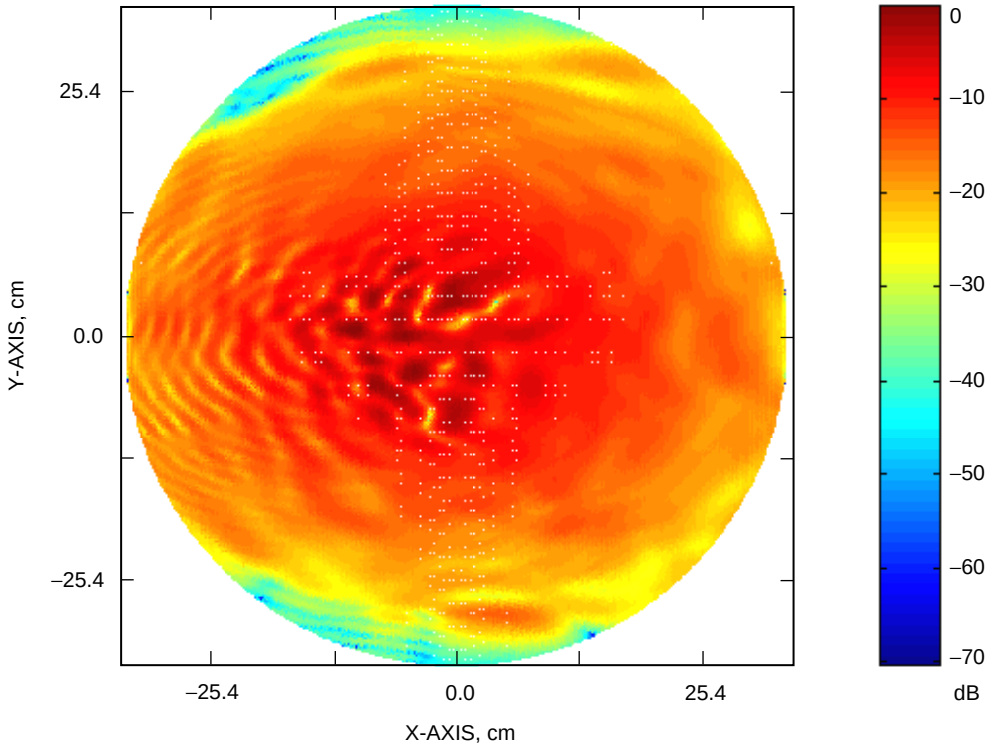

Fig. 13. Mirror current amplitude due to plane wave, nominal distortion tripled.

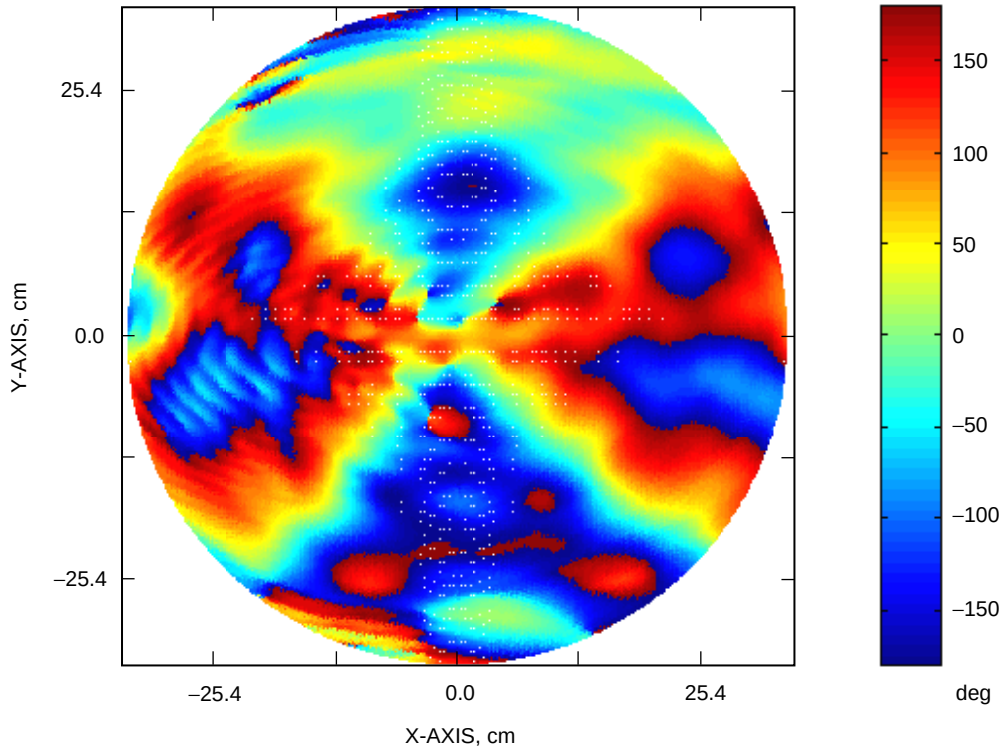

Fig. 14. Mirror current phase error, nominal distortion tripled.

is 13.9 percent; the maximum efficiency is 27.5 percent for 4 actuators, 60.3 percent for 12 actuators, 71.7 percent for 32 actuators, 79.4 percent for 52 actuators, and 69.1 percent for the existing 16-actuator plate; and the theoretical maximum efficiency is 93.1 percent.

The next results are based upon recently measured surface distortions for DSS 43 versus elevation angle. The main-reflector distortion was measured at several elevation angles and then used to predict the surface distortion from 10 to 80 deg at an interval of 10 deg using the method described in [6]. The 70-m-diameter distortion was then scaled to 34-m and placed on the DSS-13 main reflector. Scaling the distortion to 34 m allows the use of the same geometry and data files as for the previous examples. This saves computation time relative to a complete 70-m calculation and allows for direct comparison with the previous 34-m results.

Figure 15 shows the computed distortion at an elevation angle of 80 deg. The triangular grid used to create the plot is also shown. For the plot, each vertex is at the location of a measured data point, and linear interpolation is used. For the actual calculations presented next, simple closest-point interpolation was used. Since these distortions are based directly on raw measured data, many higher-order features are present that would be smoothed out if, for example, a low-order Jacobi–Bessel or Zernike expansion of the current were used, as in the previous example (Fig. 2).

By squaring the voltage coupling efficiency and correcting for any spillover before or after the deformable mirror, we may compute the antenna aperture efficiency. Figure 16 shows the antenna efficiency versus elevation angle when various deformable-mirror systems are used to correct the distortion. Figure 17 shows the corresponding gain loss in dB.

The antenna efficiency curve for the flat mirror shows a peak efficiency of around 29.6 percent near 40-deg elevation. The efficiency drops to 17.3 percent at 10 deg and 10.6 percent at 80 deg, representing gravity losses of 2.3 and 4.5 dB relative to the rigging angle. The theoretical maximum antenna efficiency

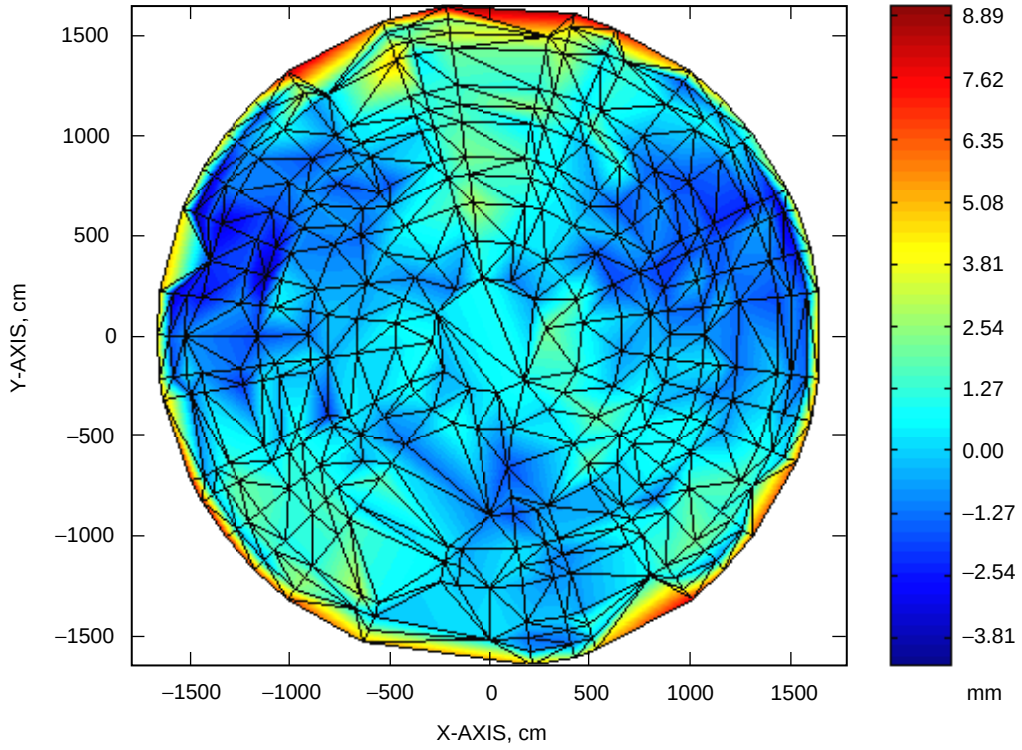

Fig. 15. The 70-m antenna distortion at 80-deg elevation, based on measured data.

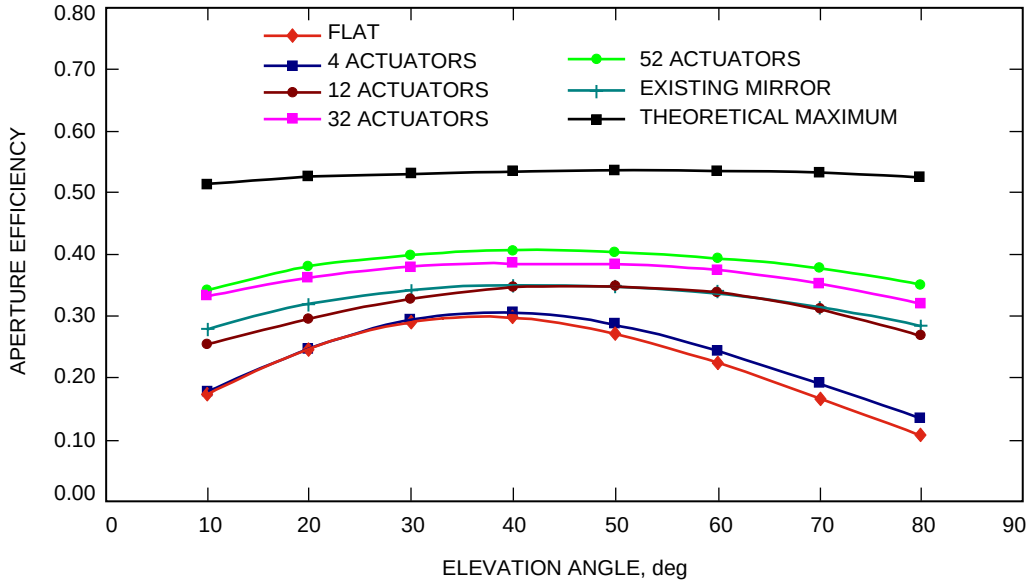

Fig. 16. Voltage coupling efficiency versus elevation angle for various deformable mirrors.

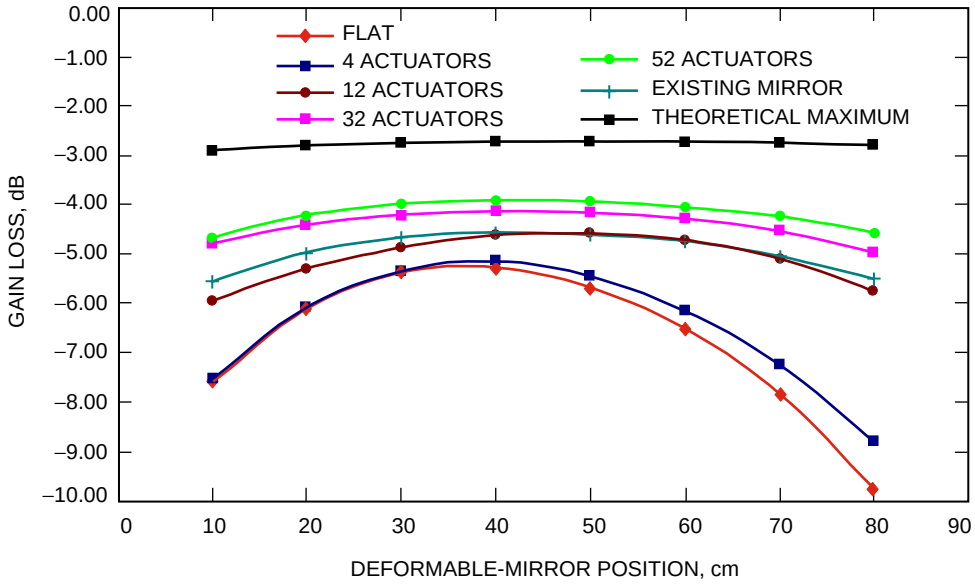

Fig. 17. Antenna aperture efficiency versus elevation angle for various deformable mirrors.

using an ideal deformable mirror is limited to approximately 52 percent for all elevation angles. This limit is due to plane-wave spillover past the subreflector (2.3 percent), ellipse (23 percent), and plane-wave and feed spillover past the deformable mirror (14 percent). The remainder of the inefficiency is due to amplitude mismatch. The spillover is caused by components of the surface distortion with short periods that scatter energy at angles larger than those covered by the subreflector or ellipse. This scattered energy is unavailable to even the theoretically ideal deformable mirror. The only way to recover this loss in efficiency is to reset the panels, correcting the error at its source, or possibly to perform the phase correction at the subreflector, where over 97 percent of the energy is still available. However, since an image of the primary mirror does not form exactly at the subreflector, there will be some coupling loss due to amplitude mismatch. Figure 17 shows that even at the rigging angle a gain improvement of over 2 dB is theoretically available by correcting those panel-setting errors with sufficiently large periods to scatter energy through the optical system onto the deformable mirror.

Figures 16 and 17 illustrate that a 4-actuator mirror is ineffective on distortions similar to those present on DSS 43. The use of 12 actuators can increase the aperture efficiency to over 25 percent across all elevation angles, an improvement of over 3.5 dB at 80 deg. As expected, increased antenna efficiency can be obtained by using more actuators, reaching at least 35 percent across all elevation angles for a 52-actuator mirror. In this case, the gain drop relative to the rigging angle due to gravity effects is reduced from 2.3 dB to 0.75 dB at 10-deg elevation and from 4.5 dB to about 0.6 dB at 80 deg. The existing deformable mirror performs roughly like a 12-actuator mirror since the actuator placement has not been optimized for the DSS-43 distortion.

This example illustrates the importance of panel setting on the overall antenna efficiency. Panel-setting errors with short periods scatter the incident plane-wave energy past the mirrors, making it unrecoverable. Panel-setting errors with longer periods are only corrected if a sufficient number of actuators are present. The relatively flat but offset curve for the 52-actuator mirror indicates that the loss due to gravity sag can be compensated quite well, but the static loss due to panel setting is of high order and not well corrected, even for a 52-actuator mirror.

VI. Conclusions

A case study of deformable-mirror performance versus actuator configuration has been performed. The DSS-13 12.7-deg distortion and the measured elevation distortions for DSS 43 have been used as examples. The simple, efficient, influence-function model for the deformable mirror allows design trade-offs to be made without the need for a detailed finite-element model of the mirror. The codes developed for this work can be used to optimize the actuator configuration for an eventual implementation on the DSN 70-m antennas, taking into account the mirror location, actuator configuration, and performance specifications.

References

[1] S. D. Slobin, *DSN/Flight Project Interface Design Handbook*, JPL 810-5, Rev. D, vol. I, "DSN Telecommunications Interfaces 70 Meter Antenna Subnet," TCI-10, Rev. G, Jet Propulsion Laboratory, Pasadena, California, January 15, 1997.

[2] P. Richter, M. Franco, and D. Rochblatt, "Data Analysis and Results of the Ka-Band Array Feed Compensation System–Deformable Flat Plate Experiment at DSS 14," *The Telecommunications and Mission Operations Progress Report 42-139, July–September 1999*, Jet Propulsion Laboratory, Pasadena, California, pp. 1–29, November 15, 1999.
http://tmo.jpl.nasa.gov/tmo/progress_report/42-139/139H.pdf

[3] M. Brenner, M. J. Britcliffe, and W. A. Imbriale, "Gravity Deformation Measurements of 70m Reflector Surfaces," 23rd Annual Meeting and Symposium of the Antenna Measurement Techniques Association, Denver, Colorado, October 21–26, 2001.

[4] D. J. Hoppe, "The Sensitivity of Main-Reflector-Distortion Compensation to Deformable-Mirror Position," *The Telecommunications and Mission Operations Progress Report 42-145, January–March 2001*, Jet Propulsion Laboratory, Pasadena, California, pp. 1–13, May 15, 2001.
http://tmo.jpl.nasa.gov/tmo/progress_report/42-145/145I.pdf

[5] E. S. Claflin and N. Bareket, "Configuring an Electrostatic Membrane Mirror by Least-Squares Fitting with Analytically Derived Influence Functions," *Journal of the Optical Society of America A*, vol. 3, no. 11, pp. 1833–1839, November 1986.

[6] R. Levy, *Structural Engineering of Microwave Antennas*, New York: IEEE Press, 1996.